

Leak Detection for Gas and Liquid Pipelines by Online Modeling

Shouxi Wang and John J. Carroll, SPE, Gas Liquids Engineering

Summary

The leakage of hydrocarbon products from a pipeline not only represents the loss of natural resources, but it also is a serious and dangerous environmental pollution and potential fire disaster. Quick awareness and accurate location of the leak event are important to reduce losses and avoid disaster.

A leak-detection method using transient modeling is introduced in this paper. This method is suitable for both gas and liquid pipelines, with comprehensive consideration of the transient-flow features of compressible flows and stochastic processing and noise filtering of the meter readings. The correlations for diagnosing the leak location and amount are derived on the basis of the online real-time observation and the readings of pressure, temperature, and flow rate at both ends of the pipeline. As an online real-time system, great attention has been paid to the stochastic processing and noise filtering of the meter readings and the models to reduce the impact of signal noise. It is also essential for the robust real-time pipeline observer to have the self-study and adjustment abilities needed to respond to the large varieties of pipeline configuration, pipeline operation conditions, and fluid properties.

Real application cases are presented here to demonstrate this leak-detection method. For example, in the leak detection of a crude-oil pipeline of 34.5 km long and 219 mm (nominal diameter), this method located the leak at 16.6 km from the pipeline upstream end, which is only 0.6 km away from the actual leak location.

Introduction

When there is a leak in the pipeline, the event will transfer to both upstream and downstream along the pipeline at the acoustic velocities. As a result, the measurements at the pipeline ends will change. The different location and rate of the leak will result in different meter readings at the pipeline ends. This is why the pipeline internal thermodynamic flowing features can be used to identify the appearance of a leak and determine its location.

It is essential for a leak-detection method and system to be sensitive to a small leak and insensitive to the system and measurement noise. To issue reliable and accurate alarms, great efforts have been paid to the stochastic processing, filtering the noise of the meter readings and the models and reducing the impact of signal noise.

Fig. 1 shows how this method works on the system control and data acquisition system (SCADA). An online real-time pipeline observer, which will always be leakage-free, is running and putting out the expected readings for the pipeline without leakage (such as flow rates at the pipeline ends) according to the measured inputs (such as pressures and temperatures measured at the upstream and downstream ends). When there is a leakage, the observer outputs are different from the meter readings, and the discrepancies between the observer outputs and the meter measurements can be used to identify the appearance, rate, and location of the leak (Wang and Wang 1996, Wang 1998).

Because the leak-detection of this method is based on the comprehensive internal flow features of the pipeline, it can be applied to the pipeline without concern for the upstream and downstream

connections. The advantage of this method over the pressure-point-analysis method is that it continues detecting the leak during the entire time it exists. Therefore, this method has more opportunity to locate the leak accurately and issue the alarm reliably.

Leak Flow Features and Models in the Pipeline

For a random leakage event leaking at rate of M_L at location of x_L from the upstream end of the pipeline, the behavior of the fluid flow in the pipeline can be described by the following mass and momentum conservation laws (Wang and Carroll 2005, Wang and Zeng 1995):

$$\text{Mass: } \frac{\partial(\rho A)}{\partial t} + \frac{\partial(vA\rho)}{\partial x} + M_L \cdot \delta(x - x_L) = 0, \dots\dots\dots (1)$$

$$\text{Momentum: } \rho \frac{\partial v}{\partial t} + \rho v \frac{\partial v}{\partial x} + \frac{\partial P}{\partial x} + g\rho \frac{dz}{dx} + \frac{\rho f v^2}{2d} = 0, \dots\dots\dots (2)$$

where the density function specifies the location of the leakage and is defined as:

$$\delta(x - x_L) = \frac{d\sigma(x - x_L)}{dx} = \begin{cases} 0, & x \neq x_L \\ \infty, & x = x_L \end{cases}, \dots\dots\dots (3)$$

$$\sigma(x - x_L) = \begin{cases} 0, & x < x_L \\ 1, & x \geq x_L \end{cases}, \dots\dots\dots (4)$$

where σ is the Heaviside unit step function.

When there is no leak in the pipeline, M_L is zero, and the model reduces to the model for normal flow without a leak.

Eqs. 1 through 4 describe the pipeline flow with a precise leakage, and they can be used to accurately simulate the impacts of a leak on the parameters at the pipeline ends. But it is impossible, according to current mathematical achievements, to find directly the reverse solution (the leak location x_L and leak rate M_L) by the above partial-differential equations with the measured pressures, flow rates, and temperatures at the two ends of the pipeline.

In the model, energy conservation is neglected because it does not help with leak detection; the leak affects only the downstream temperature at the fluid flowing speed. However, the measured temperatures are useful to estimate the flowing thermodynamic properties and calibrate the heat-transfer features of the pipeline.

It should be mentioned that this model is only for the pipeline flow in single-phase gas or liquid. Modeling multiphase flow is much more complex, and the modeling accuracy is not sufficient to be used in pipeline-leak detection. Here, only single-phase gas or liquid flow is discussed.

Diagnosing and Locating of the Leak Event

When there is a fully developed leak in the pipeline, the pipeline-pressure and mass-flow-rate profiles will be like the solid blue and red lines in the **Fig. 2**. With the measured pressures at the pipeline ends as the inputs, the pipeline model will consider the pressure profile as the dashed blue line (without leak) and estimate a flow rate (the dashed red line). Apparently, the mass-flow-rates estimated by the pipeline observer are different from the flow rates measured at the pipeline ends. The mass flow rate discrepancies between the measured and observed rates at the two pipeline ends will change with the leak rate and location, which will help diagnose, locate, and rate the leak.

Thus, the pipeline-leak-detection system can be designed as shown in **Fig. 3**. The online real-time observer picks the measured pressures as system inputs and estimates the mass flow rates for

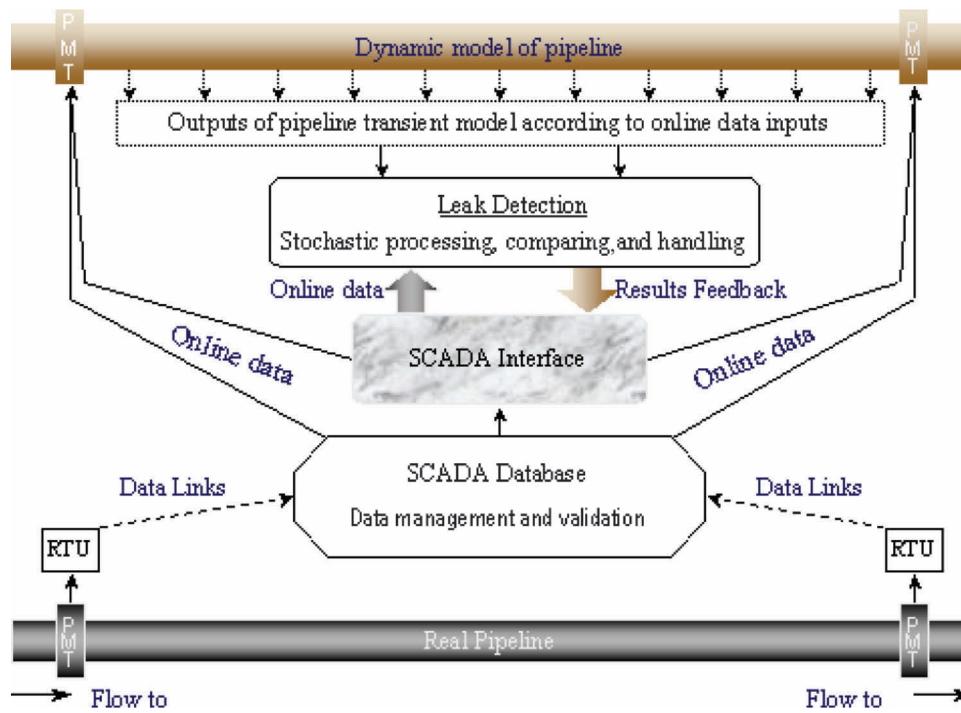


Fig. 1—Typical architecture of the leak-detection system.

the pipeline at normal flow without leak. The discrepancies of mass flow rate at time j between the measured and observed rates are defined as

$$e^j = \{e_i(j), i = 1, 2\} = \begin{cases} e_1(j) \\ e_2(j) \end{cases} = \begin{cases} M_0^j - \bar{M}_0^j \\ M_n^j - \bar{M}_n^j \end{cases} \dots \dots \dots (5)$$

The discrepancies are 0 when there is no leak. When a leak occurs, the measured mass flow rates will be different from those observed. For the leak case described in Eq. 1, the leak position is constant, and a uniform density function can be defined as (Antoniadis 1994, Antoniadis and Pham 1998, Birgé and Massart 1998)

$$f(x) = \frac{1}{L} \dots \dots \dots (6)$$

Assuming the observer gives accurate results, the discrepancies will appear and change only with the occurrence of a leak, leak rate, and location. The discrepancies of mass flow rate between the measured and observed rates can be calculated with the following equations:

$$e_1(t) = \int_{-\infty}^t \int_0^{x_L} f(x) \cdot M_L(s) \cdot ds \cdot dx, \dots \dots \dots (7)$$

$$e_2(t) = \int_{-\infty}^t \int_L^{x_L} f(x) \cdot M_L(s) \cdot ds \cdot dx. \dots \dots \dots (8)$$

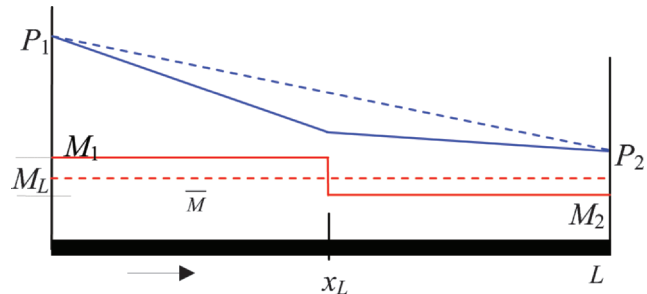


Fig. 2—Pipeline leak profiles.

Because $f(x)$ is the density function, the integration is the mean value of the random variables over the period of time. Eqs. 7 and 8 can be expressed in the following forms:

$$E[e_1(t)] = \frac{x}{L} E[M_L(t)], \dots \dots \dots (9)$$

$$E[e_2(t)] = \frac{x-L}{L} E[M_L(t)]. \dots \dots \dots (10)$$

Because the leak is identical, by comparing Eqs. 9 and 10 and using discrete processing of the SCADA-based data, the leak can be located with the following equation:

$$x_L^j = \frac{L}{1 - E(e_1^j)/E(e_2^j)}, \dots \dots \dots (11)$$

where j is the index of the time with respect to scanning and processing of the data. For each turn of run-time data, the leak location will be updated. The estimated leak position changes ran-

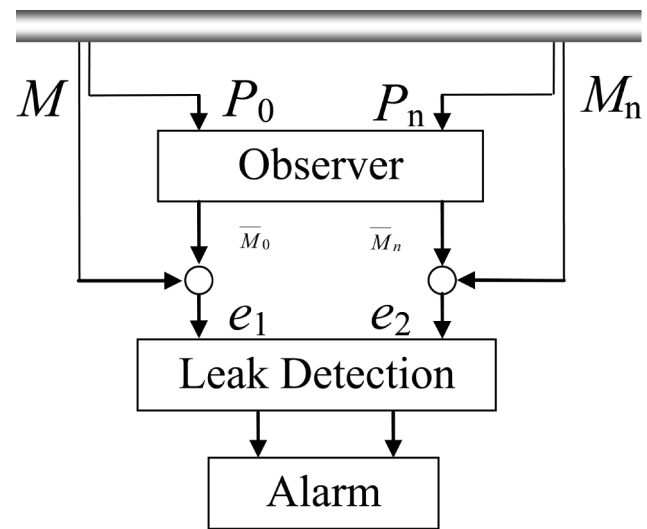


Fig. 3—Detect structure.

domly and violently if there is no leak. Now that a leak has occurred, the calculated leak position will converge and approach the actual value rapidly and keep the value constant while the leak exists.

The occurrence of a leak can be diagnosed theoretically by Eq. 12, and leak rate can be calculated with Eq. 13.

$$E(e_1^j)/E(e_2^j) = \begin{cases} <0, & \text{leak} \\ \geq 0, & \text{no leak, normal flow} \end{cases}, \dots\dots\dots (12)$$

$$M_L^j = E(e_1^j) - E(e_2^j), \dots\dots\dots (13)$$

where E is the mathematic expectation of the discrepancies over a period of time.

Real-Time Online Pipeline Observer (Wang 1998)

According to the preceding analysis, the features of the online real-time pipeline observer have a great impact on the behavior of the leak-detection method defined by the Eqs. 11 through 13. Therefore, a robust transient-flow model is essential to make the leak-detection system function properly.

Fig. 4 shows that dividing the pipeline by Δx and the time by Δt , then applying the difference quotient to the central point of each grid, the pipeline flow can be modeled with Eq. 14:

$$\left\{ \begin{array}{l} \text{State Variable:} \\ X = \{M_0, P_0, M_1, P_1, \dots, M_{n-1}, P_{n-1}, M_n, P_n\}^T \\ \text{State Equation:} \\ X^{j+1} = F(X^j, U^{j+1}) \\ \text{System Input:} \\ U^{j+1} = \{P_0^{j+1}, P_n^{j+1}\}^T \\ \text{System Output:} \\ Y^{j+1} = \{M_0^{j+1}, M_n^{j+1}\}^T \end{array} \right., \dots\dots (14)$$

where subscript n is the grid index from 0 to n , and the superscript j is the time index.

Eq. 14 is a system of $2n$ nonlinear algebraic equations with $2(n+1)$ state variables. With the two measured pressures as the system inputs, the model will estimate the mass flow rates for both pipeline ends based on the previous system state. The details of the model can be found in the Appendix. The iteration process and correlation from time to time are essential for the online real-time application to reduce the calculation time spent. Filtering must be applied to reduce and possibly eliminate the impact of noise on the meter readings and state equations.

While applying the transient model to the real pipeline system, stochastic processing and proper filtering philosophy must be applied to reduce or avoid a false alarm. The measurement noise and the state inaccuracy of numerical processing of the pipeline transient model will result in inaccurate locating and mixing of the noise with the small leak event. Usually, the moving-window method is used to filter the measurement noise. For the filtering of the nonlinear system of the pipeline online transient model, a method based on optimization and least-square theory was introduced to reduce the effect of the measurement and equation noise (Wang and Wang 1996). Besides, a close look at the measurement noise level and the adequate setting of the leak-detection threshold are important to reduce or avoid a false alarm.

Auto Study and Self-Adjusting of the Model

The online pipeline leak detection depends on the real-time pipeline simulation and requires a pipeline observer. However, it is difficult to describe the pipeline precisely and configure the pipeline model accurately because of the complexity of the pipeline layout and fittings. Moreover, the pipeline internal condition is subject to change quickly or slowly with time and operating conditions, such as the reduction in the effective pipeline diameter because of the water sediment in the pipeline. All of the above will result in a model that is a mismatch to the real pipeline being monitored.

The self-adjusting nature of the model based on the measurements of the pipeline is valuable to ensure that the transient model

always matches the real pipeline and that the observer is performing well.

Eq. 14 can be an online model for both a pipeline observer and a parameter trainer. When it works as a parameter trainer, it can be converted to following forms:

$$\begin{cases} X = \{M_0, P_0, M_1, P_1, \dots, M_{n-1}, P_{n-1}, M_n, P_n\}^T \\ X^{j+1}(\theta) = F(X^j, U^{j+1}, \theta) \\ U^{j+1} = \{P_0^{j+1}, P_n^{j+1}\}^T \\ Y^{j+1} = hX^{j+1} \end{cases}, \dots\dots (15)$$

where θ is the vector of the parameters to be studied, and h is the transform matrix of the system variables and system outputs:

$$h = \begin{Bmatrix} 1, & 0, & \dots, & 0 \\ 0, & \dots, & 0, & 1 \end{Bmatrix}, 2(n+1) \times 2. \dots\dots (16)$$

If the observer defined by Eq. 15 gives the simulation results as \bar{Y} , the discrepancies between the measured and observed can be defined as follows:

$$e^j = Y^j - \bar{Y}^j = Y^j - h\bar{X}^j = \begin{Bmatrix} M_0^j - \bar{M}_0^j \\ M_n^j - \bar{M}_n^j \end{Bmatrix}. \dots\dots (17)$$

Considering that the discrepancies are caused only by the inaccuracy or small changes of parameters θ , the θ can be trained or studied with following procedure (Huang and Liu 1993):

$$\begin{cases} \theta^j = \theta^{j-1} - \Delta\theta^j, & \Delta\theta^j = (C_j^T C_j)^{-1} C_j^T e^j \\ C_j = \begin{pmatrix} h \frac{\partial \bar{X}_m^j}{\partial \theta_i} \end{pmatrix}, & m = 0, 1, \dots, 2(n+1), \dots\dots (18) \\ & i = 1, 2, \dots, r; j \geq r \end{cases}$$

where r is the number of parameters to be studied, or the size of vector θ , $\frac{\partial \bar{X}_m^j}{\partial \theta_i}$ is the sensitivity of the m th system variable to the i th parameter at the j th sampling, and C_j is a matrix of the sensitivity.

While there is enough scanning and measurements ($j \geq r$), Eq. 18 can be used to iterate and train the parameters. The configuration parameters of the pipeline online model will be adjusted to the trained parameters that will keep the online model matching the real pipeline flowing conditions. The most common parameters required to be trained in the pipeline leak detection are the pipeline internal diameter and the constant-flow-rate bias between the upstream and downstream flow meters.

It must be mentioned that the training process of parameters can be applied only on the period of measurement when there is no leak in the pipeline. The training process uses Eq. 18 to find the best parameters for the least discrepancy of measured and observed flows over that training period. The parameters to be adjusted are effective internal diameter and overall-heat-transfer coefficient. The equivalent pipeline length is an alternative of internal diameter to achieve match. But, it is not applicable in leak detection because of its side effect on leak location. The constant-measurement bias of the flow meter is also obtained through the training process to adjust the discrepancies of measured and observed flow rates.

Applications and Discussions

Crude-Oil Pipeline. Fig. 5 shows the pressure and flow-rate trends measured at the upstream and downstream ends of the Caheji-Renqiu pipeline, Huabei oil field of PetroChina, on 11 August 2001. The temperatures were almost constant at 65.2°C at upstream and 45.7°C at downstream. The measurements were taken with pressure transmitters of 0.2% accuracy, vortex meters of 2% accuracy, and temperature transmitters of 1% accuracy. The pipeline has an outside diameter of 219 mm [internal diameter (ID)=205 mm] and transports crude oil more than 34.5 km.

A leak happened on this pipeline at 0:49:12 11 August 2006, as shown in Fig. 5 which shows the trends of measured pressures and flow rates at the two pipeline ends. In this case, the two pressure trends dropped and the two flow rate trends went apart suddenly after approximately 25 seconds of the leak start, which can be estimated approximately by the times the trends changed, the

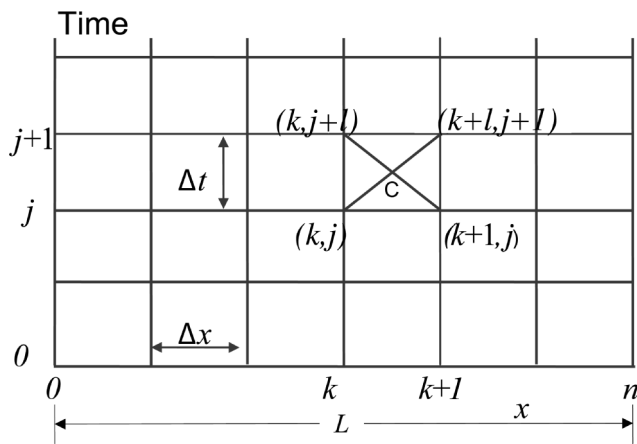


Fig. 4—Pipeline grid.

acoustic velocity along the pipeline, and the compensation of time used in the noise filtering. From the trends, we can see that the flow reaches its new balance very quickly.

By setting the simulation interval at 2 seconds and the pipeline grid size at 1 km, the pipeline observer gave an estimation of the flow rates at both ends with the measured pressures as the inputs. The flow-rate trends of the measured and observed rates are shown on Fig. 6, which gives three pairs of flow rates: the measured flow rates, the observed flow rates without model adjusting and parameter training, and the observed flow rates from the trained observer.

Before the observer is trained, it uses the original configuration to set up its transient model. It is difficult to make all the pipeline configuration and fluid properties as accurate as required. It is more difficult to keep the flowing and fluid in the same condition as defined originally. As a result, the observer without training, will give the flow rates far away from the actual flow (depending on how accurate the original configuration is) as shown by M_0 and M_n in Fig. 6. Apparently, in the case of Fig. 6, the observed flow rates can not help Eq. 11 to alarm the appearance of the leak and locate the leak. After training the model with the latest run time data without leakage for the effective internal diameter and constant meter bias, a new pipeline internal diameter of 182.455 mm was obtained. After replacing the original internal diameter of 205 mm with the new adjusted value, the online transient model gave the flow rates as M_0 and M_n in Fig. 6. From the trends, we can see that the trained pipeline observer matches the normal flows without leaks very well, and the signal noise are significantly removed.

At the given interval (2 seconds for this case) the pipeline observer took the SCADA data and simulated the flow rates. The flow rates observed were then used in Eq. 11, and the leak position was calculated, as shown as the blue and green lines in Fig. 7.

While there is no leak, the calculated leak location varies randomly and violently. When a leak occurs, the calculated leak location keeps a constant value after a short period of violent changes and approaching procedure. Now that the change of the estimated leak location is in the given changing band for a while, a leak alarm can be issued with the detected leak location as the value of the horizontal section. In Fig. 7, the “actual” red line specifies when the leak actually started and where the actual leak is located (17.2 km from the upstream end). In this case, a leak at 15.75 km was detected as shown as the “detected” blue line, which comes from the locating process without the compensation of the constant measurement bias of the flowmeters. The constant measurement bias between the upstream and downstream flowmeters also influences the leak location. After modifying the constant meter bias with -1.15219 kg/s obtained from the online training, a better leak location of 16.6 km was given, as shown in the “modified” green line in Fig. 7.

There is approximately a 3-minute delay before a leak alarm can be announced in this case. The time required for detecting and approaching the leak location is different from case to case depending on the pipeline configuration, fluid characteristics, flowing conditions, and leak location and rate.

Figs. 8 through 10 demonstrate the trends of real flow and the leak-detection process for the leak test case that occurred on 21 December 2000 on the same pipeline. The actual leak was at 11.2 km from the upstream end. There are two occurrences of leaks, and the leak rate is approximately 2.0 kg/s, which is close to the flow-measurement noise and meter bias.

Fig. 8 shows the pressure and flow-rate readings measured at the pipeline ends. Fig. 9 shows the measured flow rates (M_0 and M_n) and the observed flow rates (M_0 and M_n). The internal diameter of the pipeline model was adjusted to 183.922 mm by online training.

The “actual” red line in Fig. 10 shows the actual leak positions and durations. The blue line is the detected leak location without compensation of the constant meter bias, which was -0.5823 kg/s (studied from the run-time data without leak). The green line is the leak-location procedure after training and meter bias compensation. Although it changes violently with the noise and flows, the detected leak location approaches the actual leak position while the leak exists.

In this case, the approaching and convergence of the leak location are not as good as the case in Fig. 5 because the leak rate is close to the flow meters’ noise level and the constant meter bias. For the first leak of this case, the leak lasted only 5 minutes, and there was not enough time for the leak-detection procedure to reach and converge completely to the leak position.

Simulated Leak Case for a Natural-Gas Pipeline. Fig. 11 shows the pressure and flow-rate trends at the upstream and downstream

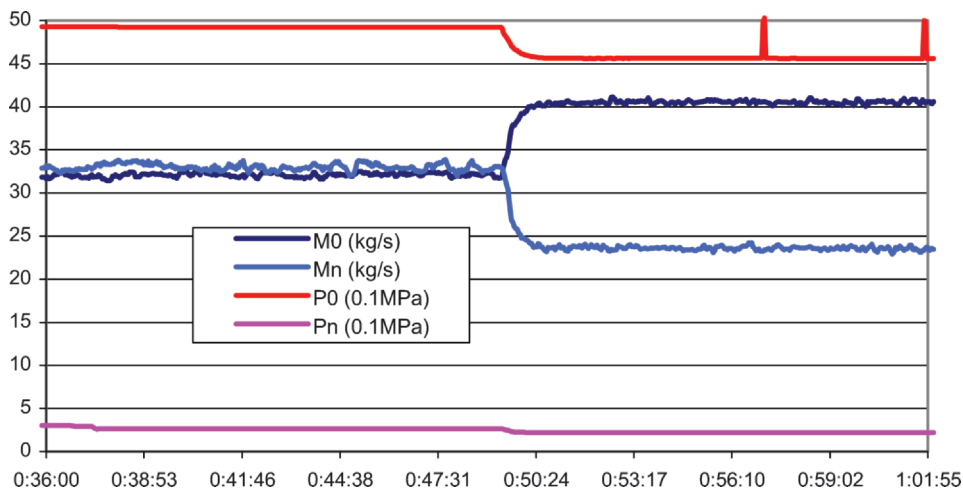


Fig. 5—Measurement trends (11 August 2001).

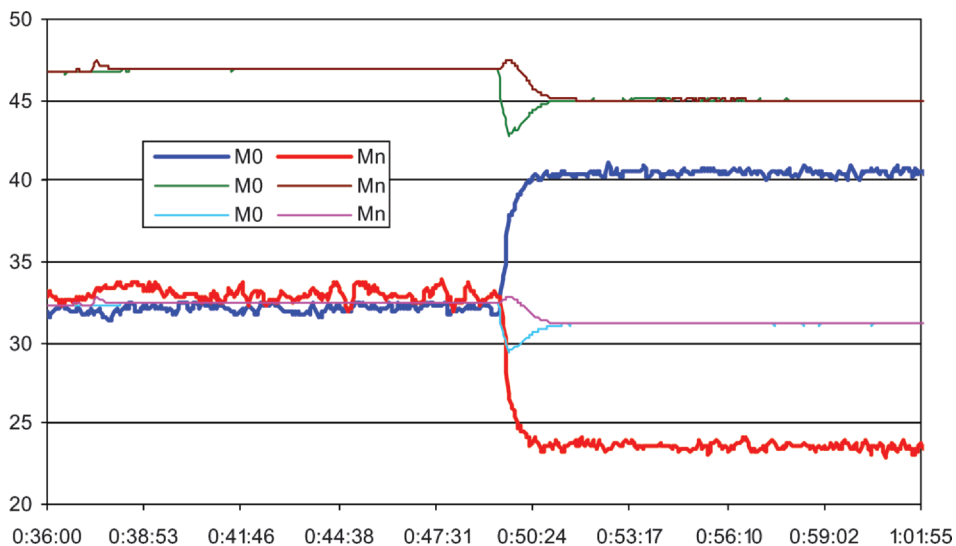


Fig. 6—Measured and observed flow rates (kg/s).

ends of a natural-gas pipeline for two leak occurrences simulated by the pipeline online observer. The pipeline has an inside diameter of 90 mm and a length of 35 km. The time interval is set to 30 seconds for both leak simulation and detection. The two occurrences leaked at different locations and at the same rate of 45.12 std m³/h, which is approximately 4.1% of the normal flow without leak. The first leak began at 3:34:30 and ended at 12:12:00, occurring 20 km from the upstream end. The second leak was 15 km from the upstream end, and it started at 16:45:00 and ended at 5:26:30 the next day.

Fig. 12 shows the location and duration of the actual leaks and the leak-detection procedure. It takes more time to locate leaks in the gas pipeline compared to the liquid pipeline because the leak influence takes more time to reach the pipeline ends.

Simulated Leak Case for Acid-Gas Pipeline. Fig. 13 shows the pressure and flow-rate trends at the upstream and downstream ends of an acid-gas pipeline for a leak occurrence simulated by the pipeline online observer. This 3-in. pipeline transfers the acid-gas over 4 km to the injection well in a Bigoray field acid-gas-injection system (Wang and Carroll 2005). The acid gas consists of 9% H₂S, 88% CO₂, 2% water, and 1% C₁₊. The simulated leak occurred 2 km from the upstream end of the pipeline from 0:33:20 to 1:58:20, with a leak rate of 0.2 kg/s, which is approximately 2% of the normal flow rate.

Fig. 14 shows the approaching procedure of the leak detection and the actual leak location and duration. After several minutes,

the detected-leak-location trend reaches a horizontal line 2.27 km from the upstream end, which is 0.27 km away from the actual leak location.

Conclusions

According to our research and experience in pipeline leak-detection technologies and systems, the following conclusions can be drawn:

1. Among the pipeline leak-detection technologies and methods, leak detection by the transient model makes the best use of all pipeline flowing characteristics and the SCADA data. It can be applied to large varieties of circumstances because it is based on the comprehensive pipeline internal flowing features.
2. The behavior of the leak detection by online models depends on the performance of the pipeline online observer. The online self-adjustment is an essential function of the online observer to ensure that the transient model actually represents the pipeline and flows being monitored. The online calibration of the transient model (with the parameters from the online study) is the comprehensive solution to the inaccuracies and uncertainties of the pipeline configuration, fluid properties, and flowing conditions.
3. False and inaccurate alarms are always of great concern for a diagnostic system. Stochastic processing and proper filtering philosophy must be applied to the pipeline leak-detection procedure to ensure that it is sensitive to small leaks and insensitive to signal and system noise. A close look at the measurement-noise level and the adequate setting of the leak-detection threshold are important to reduce or avoid false alarms. The leak-

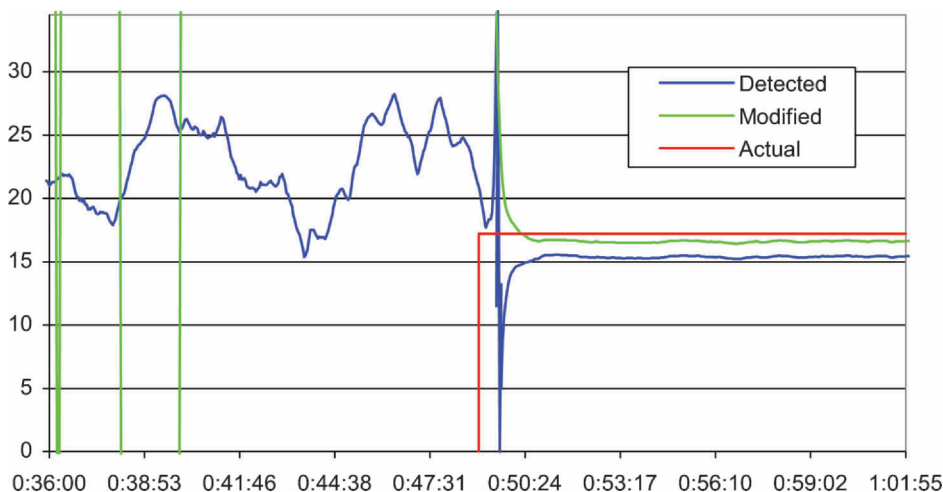


Fig. 7—Leak location (km).

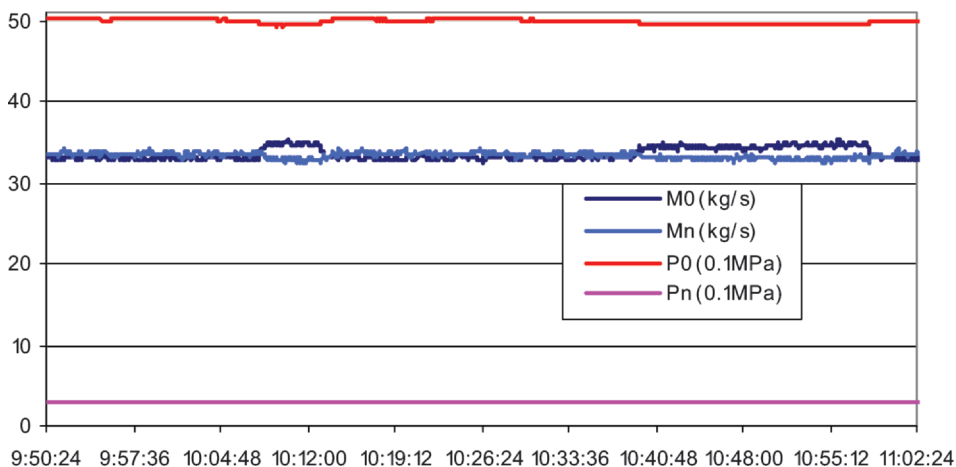


Fig. 8—Measurement trends (21 December 2000).

detection expectation is also a big implementation issue. The smaller the leak you want to be noticed, the more frequently the false alarms will occur.

4. The qualities of the measurements have great impact on how fast the leak can be found and how small the leak can be. Calibration procedures for finding the critical features of the system being monitored are essential, such as the noise level of the measurements. The leak rate, leak duration, measurement noise and bias, and the setting of the minimum leak to be detected also affect the required detection time as well.
5. Because of the compressibility of gas, the leak impacts on a gas pipeline are not as fast and significant as on a liquid pipeline. The changes of the measured run-time data caused by the leak are slower and smaller, which will increase the processing time of the leak detection. If the leak is too small, the instruments at the pipeline ends may not even notice the changes, and the changes will be hidden in the noise. Certainly, more-accurate meters and instrumentation will provide a better solution. Regardless, a simulation of different leak scenarios will help determine the smallest leak that can be detected for a specific pipeline.

Nomenclature

A = flow area of the pipeline, m^2
 C_j = matrix of sensitivity to parameters
 D = inside diameter of the pipeline, m
 E = vector of mass-flow-rate discrepancies
 e_1, e_2 = discrepancies between measured and observed mass

flow rates at up and downstream ends of pipeline, respectively, kg/s
 f = Darcy friction factor
 g = acceleration due to gravity, m/s^2
 h = conversion matrix of system variables and outputs
 L = length of the pipeline, m
 M = mass flow rate, kg/s
 M_0 = mass flow rate measured at upstream end, kg/s
 M_1, M_2 = upstream and downstream mass flow rates, respectively, kg/s
 M_L = leak rate, kg/s
 M_n = mass flow rate measured at downstream end, kg/s
 \hat{M} = calculated mass flow rate, kg/s
 M_o = mass flow rate observed at upstream, kg/s
 M_n = mass flow rate observed at downstream end, kg/s
 P = pressure, Pa
 P_0 = pressure measured at upstream end, Pa
 P_1, P_2 = upstream and downstream pressures, respectively, Pa
 P_n = pressure measured at downstream end, Pa
 t = time, seconds
 T = temperature, K
 U = vector of system inputs
 v = velocity, m/s
 x = coordinate along the pipeline, m
 x_L = leak location, m
 X = vector of system variables

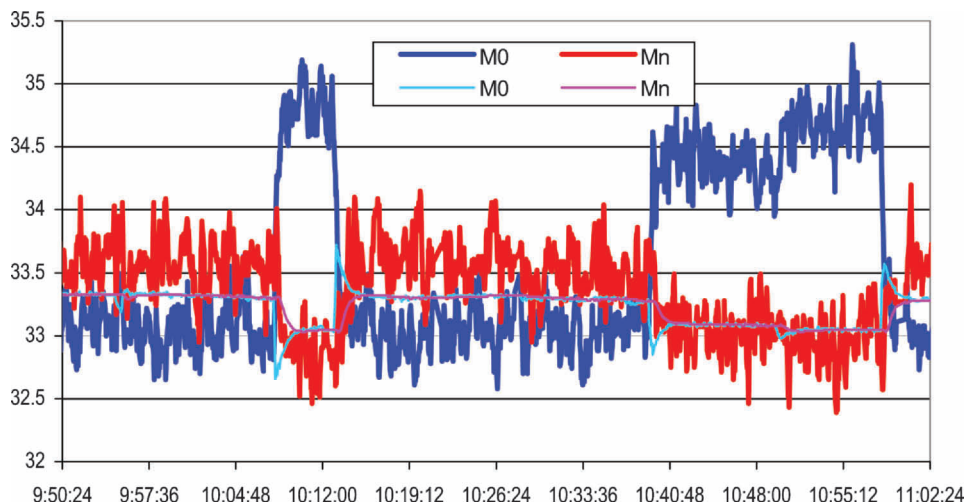


Fig. 9—Measured and observed flow rates.

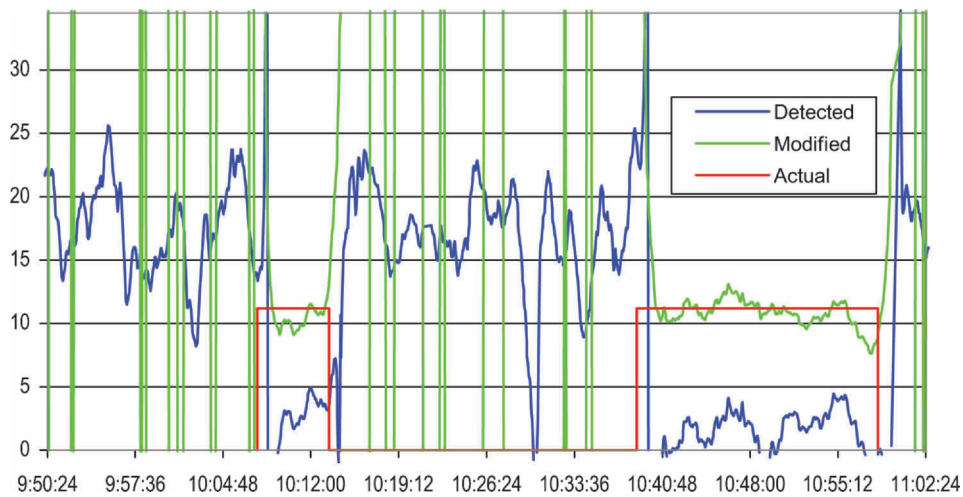


Fig. 10—Leak location (km).

Y = vector of system outputs
 Z = elevation, m
 θ = vector of parameters to be studied
 ρ = density of the fluid, kg/m³

Subscripts

$i_{1,2}$ = index of pipeline end, 1 for upstream and 2 for downstream
 j = index of time
 k = index of the pipeline grid node, from zero to n
 L = leakage

Superscripts

J = index of time

References

- Antoniadis, A. and Pham, D.T. 1998. Wavelet Regression For Random or Irregular Design. *Comp. Stat. and Data Analysis* **28**(4): 353–369.
 Antoniadis, A. 1994. Smoothing Noisy Data With Coiflets. *Statistica Sinica* **4** (2): 651–678.
 Birgé, L. and Massart, P. 1997. From Model Selection to Adaptive Estimation. In D. Pollard (ed.), *Festschrift for L. Le Cam*. Springer: 55–88.
 Huang, G. and Liu, X. 1993. *Reverse Problems of Mathematics and Physics*. Shandong Science and Technology Publisher, Shandong, China.
 Isermann, R. 1984. Process Fault Detection Based on Modeling and Estimation Methods—A Survey. *Automatica* **20** (4): 387–404.

- Liou, C.P. 1991. Leak Detection and Location by Transient Flow Simulations, *Proc., API Pipeline Conference*, Dallas, 23 April.
 Van Reet, J.D. and Skogman, K.D. 1987. The Effect of Measurement Uncertainty on Real Time Pipeline Modeling Applications. ASME Pipeline Engineering Symposium.
 Wang S. 1998. Leak Detection System for Oil and Gas Pipelines (Ph.D thesis), Southwest Petroleum U., Nanchong, China.
 Wang, S. and Carroll J.J. 2005. Profiles for Acid Gas Injection Wells. Proc. 55th Canadian Chemical Engineering Conference, Toronto, Canada, 16–19 October.
 Wang, S. and Wang, J. 1996. *Pipeline Automation*. Petroleum Industry Publisher of China, Beijing, 3–6 June.
 Wang, S. and Zeng, Z. 1995. The Method and Software of Steady and Unsteady Simulations of Natural Gas Pipeline Networks, *Natural Gas Industry* **15** (2).

Appendix—Pipeline Online Transient Model

For the system of Eq. 14, applying the difference quotient to the central point of each grid in Fig. 4, the pipeline transient flow can be modeled as shown below:

$$\begin{cases} X = \{M_0, M_1, P_1, \dots, M_{n-1}, P_{n-1}, M_n\}^t \\ X^{j+1} = [J_1^j]^{-1} \{-J_2^j X^j + S_1^j U^{j+1} + S_2^j U^j\} \\ U^{j+1} = \{P_0^{j+1}, P_n^{j+1}\}^t \\ \bar{Y}^{j+1} = \{\bar{M}_0^{j+1}, \bar{M}_n^{j+1}\}^t = \begin{Bmatrix} 1 & 0 & \dots & 0 \\ 0 & \dots & 0 & 1 \end{Bmatrix} X^{j+1} \end{cases}, \dots \text{ (A-1)}$$

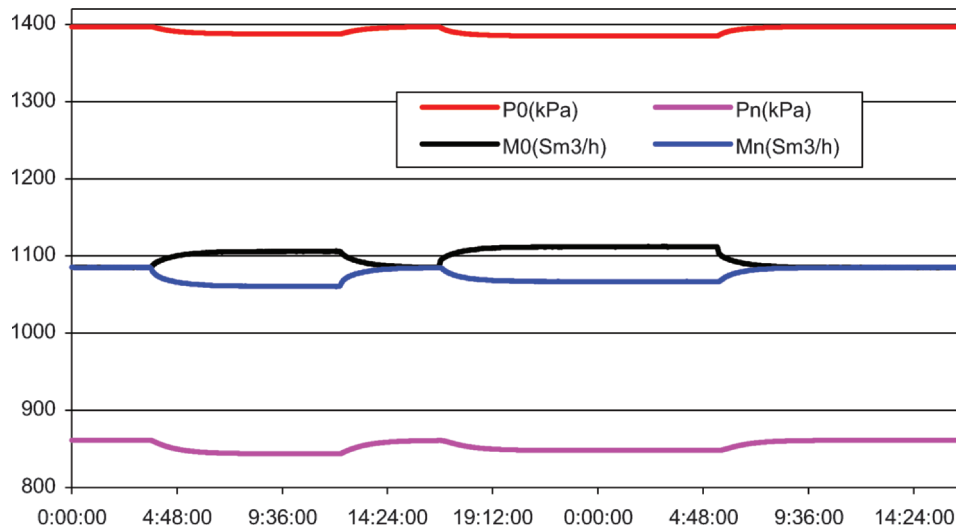


Fig. 11—Simulated leak trends (natural gas).

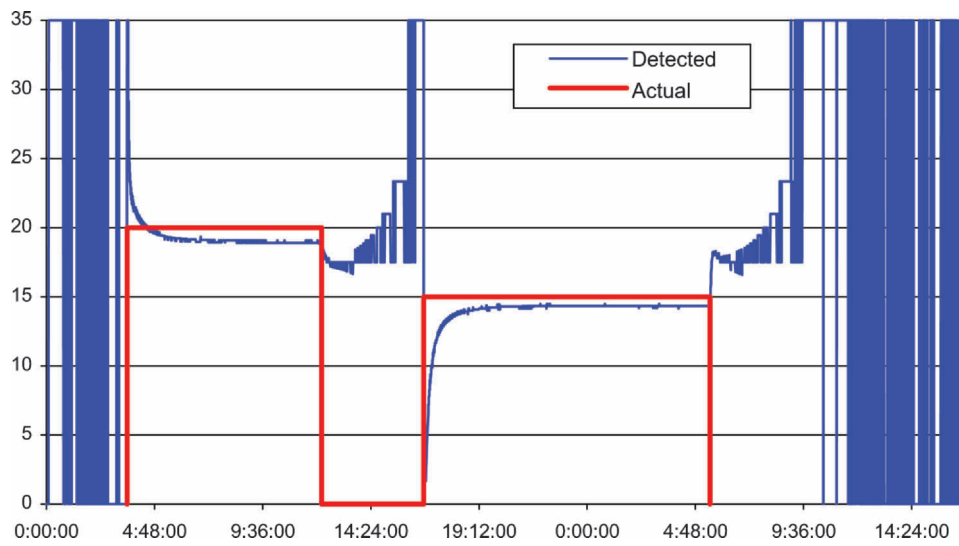


Fig. 12—Leak location (km, natural gas).

where subscript is the grid index from 0 to n , and the superscript j is the time index.

The matrices related to the calculation are listed below (Eqs. A-2 to A-10):

$$J_i^j = \begin{bmatrix} [J_{i0}^j] & 0 & \dots & 0 & \dots & 0 & 0 \\ 0 & [J_{i1}^j] & \dots & 0 & \dots & 0 & 0 \\ & & \vdots & & \vdots & & \\ 0 & 0 & \dots & [J_{ik}^j] & \dots & 0 & 0 \\ & & \vdots & & \vdots & & \\ 0 & 0 & \dots & 0 & \dots & [J_{in-2}^j] & 0 \\ 0 & 0 & \dots & 0 & \dots & 0 & [J_{in-1}^j] \end{bmatrix}, \quad \begin{cases} 2n \times 2 \\ k = 0, 1, \dots, n-1 \\ i = 1, 2 \end{cases} \quad \text{(A-2)}$$

$$[J_1]_0^j = \begin{bmatrix} -B_0^j & 1 & B_0^j \\ C_0^j - E_0^j & G_0^j + 1 & C_0^j + E_0^j \end{bmatrix}, \quad \text{(A-3)}$$

$$[J_2]_0^j = \begin{bmatrix} -B_0^j & -1 & B_0^j \\ R_0^j - E_0^j & G_0^j + 1 & R_0^j + E_0^j \end{bmatrix}; \quad \text{(A-4)}$$

$$[J_1]_{n-1}^j = \begin{bmatrix} 1 & -B_{n-1}^j & B_{n-1}^j \\ G_{n-1}^j - 1 & C_{n-1}^j - E_{n-1}^j & C_{n-1}^j + E_{n-1}^j \end{bmatrix}, \quad \dots \quad \text{(A-5)}$$

$$[J_2]_{n-1}^j = \begin{bmatrix} -1 & -B_{n-1}^j & B_{n-1}^j \\ G_{n-1}^j - 1 & R_{n-1}^j - E_{n-1}^j & R_{n-1}^j + E_{n-1}^j \end{bmatrix}, \quad \dots \quad \text{(A-6)}$$

$$[J_1]_k^j = \begin{bmatrix} 1 & -B_k^j & 1 & B_k^j \\ G_k^j - 1 & C_k^j - E_k^j & G_k^j + 1 & C_k^j + E_k^j \end{bmatrix}, \quad \dots \quad \text{(A-7)}$$

$$[J_2]_k^j = \begin{bmatrix} -1 & -B_k^j & -1 & B_k^j \\ G_k^j - 1 & R_k^j - E_k^j & G_k^j + 1 & R_k^j + E_k^j \end{bmatrix}, \quad \dots \quad \text{(A-8)}$$

$$S_1^j = \begin{bmatrix} 1 & G_0^j - 1 & 0 & \dots & 0 & 0 & 0 \\ 0 & 0 & 0 & \dots & 0 & 1 & G_{n-1}^j + 1 \end{bmatrix}^t, \quad 2n \times 2, \quad \dots \quad \text{(A-9)}$$

$$S_2^j = \begin{bmatrix} -1 & G_0^j - 1 & 0 & \dots & 0 & 0 & 0 \\ 0 & 0 & 0 & \dots & 0 & -1 & -I_1 + \bar{V}_{n-1}^j + 1 \end{bmatrix}^t, \quad 2n \times 2 \quad \dots \quad \text{(A-10)}$$

where $I_1 = \Delta x / \Delta t$.

Each element of the matrices is determined from the configuration, flow, and fluid properties of the grid at the specific time.

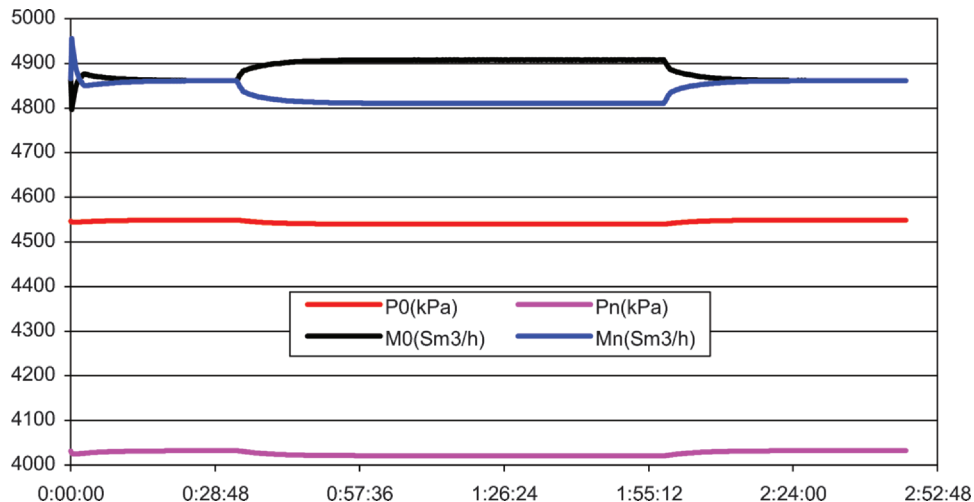


Fig. 13—Simulated leak trends (acid gas).

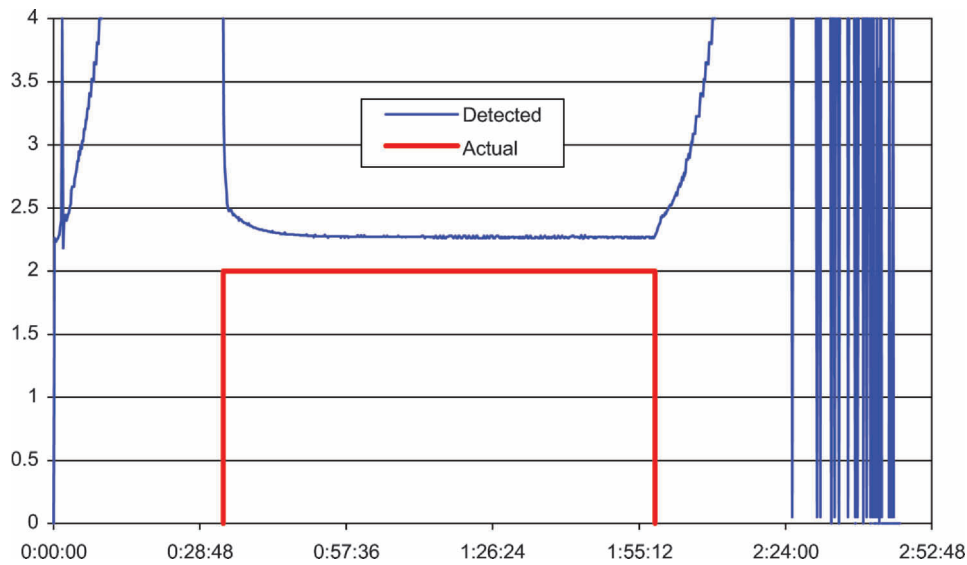


Fig. 14—Leak location (km, acid gas).

For the grid bounded by (k, j) and $(k+1, j+1)$, the related parameters can be calculated with the following equations:

$$B_k^j = \frac{\Delta t}{\Delta x} \left(\frac{a}{A} \right)_k^j, \dots \dots \dots (A-11)$$

$$C_k^j = \frac{\Delta x}{\Delta t} \left(\frac{1}{A} \right)_k^j + \frac{\Delta x}{4} \left(\frac{f\bar{V}}{d \cdot A} \right)_k^j, \dots \dots \dots (A-12)$$

$$E_k^j = \left(\frac{\bar{V}}{A} \right)_k^j, \dots \dots \dots (A-13)$$

$$G_k^j = \frac{g \cdot \Delta x}{2} \left(\frac{1}{a^2} \cdot \frac{dz}{dx} \right)_k^j, \dots \dots \dots (A-14)$$

$$R_k^j = \Delta xy \left(\frac{f\bar{V}}{d \cdot A} \right)_k^j - \frac{\Delta x}{\Delta t} \left(\frac{1}{A} \right)_k^j, \dots \dots \dots (A-15)$$

where a is the local acoustic velocity, $\bar{\rho}$ is the average density of the grid and \bar{V} is the average flow speed of the grid. The average properties and flow speed of the grid are derived from its average flow rate, pressure and temperature, such as:

$$\bar{V}_k^j = \left(\frac{\bar{M}}{\bar{\rho}A} \right)_k^j, \dots \dots \dots (A-16)$$

The average variables of the grid can be calculated by

$$\begin{cases} \bar{M}_k^j = 0.25(M_k^j + M_{k+1}^j + M_k^{j+1} + M_{k+1}^{j+1}) \\ \bar{P}_k^j = 0.25(P_k^j + P_{k+1}^j + P_k^{j+1} + P_{k+1}^{j+1}) \\ \bar{T}_k^j = 0.25(T_k^j + T_{k+1}^j + T_k^{j+1} + T_{k+1}^{j+1}) \end{cases} \dots \dots \dots (A-17)$$

SI Metric Conversion Factors

bar × 1.0*	E+05 = Pa
°F (°F-32)/1.8	= °C
in. × 2.54*	E+00 = cm
lbm × 4.535 924	E-01 = kg
mile × 1.609 344*	E+00 = km

*Conversion factor is exact.

Shouxi Wang has more than 15 years of combined experience of engineering and software development in oil and gas handling and transportation. Wang holds a PhD degree in petroleum engineering, a MSc degree in mechanical engineering, and a BSc degree in oil and gas storage and transportation from Southwest Petroleum University in China. Wang has extensive expertise and experience in the software development of pipeline-network simulation, pipeline-leak detection and engineering applications. **John Carroll** is the director of geo-storage process engineering at Gas Liquids Engineering. Carroll is a registered professional engineer in the provinces of Alberta and New Brunswick and is a member of several professional associations including SPE. He holds a PhD degree and a BS degree in chemical engineering from the University of Alberta, Edmonton.